

# Direct recordings of grid-like neuronal activity in human spatial navigation

Joshua Jacobs<sup>1</sup>, Christoph T Weidemann<sup>2</sup>, Jonathan F Miller<sup>1</sup>, Alec Solway<sup>3</sup>, John F Burke<sup>4</sup>, Xue-Xin Wei<sup>4</sup>, Nanthia Suthana<sup>5</sup>, Michael R Sperling<sup>6</sup>, Ashwini D Sharan<sup>7</sup>, Itzhak Fried<sup>5,8,9</sup> & Michael J Kahana<sup>4,9</sup>

**Grid cells in the entorhinal cortex appear to represent spatial location via a triangular coordinate system. Such cells, which have been identified in rats, bats and monkeys, are believed to support a wide range of spatial behaviors. Recording neuronal activity from neurosurgical patients performing a virtual-navigation task, we identified cells exhibiting grid-like spiking patterns in the human brain, suggesting that humans and simpler animals rely on homologous spatial-coding schemes.**

The hippocampal formation, which includes the hippocampus and entorhinal cortex, contains a diverse array of cell types that support spatial navigation and memory. A key component of this system is the hippocampal place cell<sup>1,2</sup>, which encodes the animal's presence at a particular spatial location to support navigation and encoding of spatial memories. Place cells have been identified in various species, including rats<sup>1</sup>, mice<sup>3</sup>, bats<sup>4</sup> and humans<sup>2</sup>. Much research has focused on how place-cell representations are formed<sup>5</sup> and how place cells represent the current location without the animal receiving sensory input<sup>6</sup>. The discovery of entorhinal cortex grid and grid-by-direction cells<sup>7–10</sup> offers a possible answer to these questions by providing the hippocampus with a robust location signal that is encoded using characteristic triangular coordinates and updated with the animal's movements.

In humans, functional magnetic resonance imaging (fMRI) provides indirect support for the existence of grid cells. fMRI recordings from subjects performing a spatial object-placement task has shown that hemodynamic activity in a network of regions, including entorhinal cortex, is modulated by the direction of movement<sup>11</sup>. Notably, this directional activity exhibits sixfold rotational symmetry and therefore conforms to the 60° periodicity of the firing patterns of grid cells<sup>7</sup>. We used invasive brain recordings to provide direct electrophysiological evidence for grid-like representations in navigating primates.

To directly identify human neurons exhibiting grid-like spatial firing, we recorded single-neuron spiking activity from electrodes that

were surgically implanted in 14 patients undergoing treatment for drug-resistant epilepsy. Owing to the clinical recording equipment used for epilepsy monitoring, patients were constrained to their beds and unable to physically navigate. Instead, patients performed a virtual navigation task on a bedside laptop computer<sup>12</sup>. The task required that they navigate between four objects that were hidden at different locations in a virtual environment (Fig. 1a). Unlike some previous studies<sup>2,13</sup>, this environment was a large open square, analogous to the sizable arenas often used to record grid cells from rodents<sup>7</sup>. On each trial of the task the participant navigated to the location of a randomly selected object. Because objects were invisible, the participants were likely to use an allocentric navigation strategy based on path integration, which relies on the hippocampal formation<sup>14</sup>. Participants were successful in learning the locations of the four objects, as there was a significant decrease in their mean delivery time from 14 to 8 s over the course of each session ( $P < 0.005$ ,  $t$  test; Fig. 1b).

We identified grid-like spatial firing by measuring the firing rate of each cell across the virtual environment and testing whether the locations where individual cells activated were arranged in a sixfold-symmetric triangular grid. We measured neuronal firing according to the participant's location by dividing the square environment into a 28 × 28 array and computing the mean firing rate of each neuron for every virtual position. A number of cells exhibited increased spiking activity at multiple locations. Thus, these cells appeared to be fundamentally different from hippocampal place cells, which usually activate only at one location<sup>5</sup>.

Next, we tested whether the multiple locations at which each neuron activated were arranged in the triangular lattice structure that is characteristic of grid cells<sup>7</sup>. This allowed us to distinguish cells with

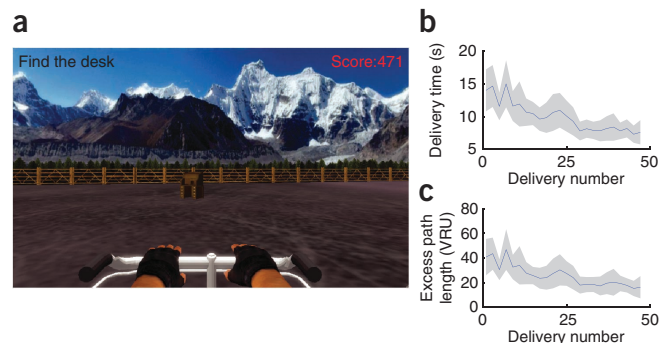


**Figure 1** Virtual navigation task. (a) Participant's view of the experiment. (b) Mean duration of successive deliveries in the task, averaged across consecutive pairs of deliveries. (c) Mean excess path length. VRU is a measure of virtual distance. Error shading denotes 95% confidence intervals.

<sup>1</sup>School of Biomedical Engineering, Science and Health Systems, Drexel University, Philadelphia, Pennsylvania, USA. <sup>2</sup>Department of Psychology, Swansea University, Swansea, UK. <sup>3</sup>Princeton Neuroscience Institute, Princeton University, Princeton, New Jersey, USA. <sup>4</sup>Department of Psychology, University of Pennsylvania, Philadelphia, Pennsylvania, USA. <sup>5</sup>Department of Neurosurgery, David Geffen School of Medicine and Semel Institute for Neuroscience and Human Behavior, University of California, Los Angeles, California, USA. <sup>6</sup>Department of Neurology, Thomas Jefferson University, Philadelphia, Pennsylvania, USA. <sup>7</sup>Department of Neurosurgery, Thomas Jefferson University, Philadelphia, Pennsylvania, USA. <sup>8</sup>Functional Neurosurgery Unit, Tel-Aviv Medical Center and Sackler Faculty of Medicine, Tel-Aviv University, Tel-Aviv, Israel. <sup>9</sup>These authors contributed equally to this work. Correspondence should be addressed to J.J. (joshua.jacobs@drexel.edu), M.J.K. (kahana@psych.upenn.edu) or I.F. (ifried@mednet.ucla.edu).

**Figure 2** Examples of grid-like spatial firing.

(a) The activity of a cell from participant 6's left entorhinal cortex. Left, overhead view of the environment, with color representing the firing rate (in Hz) at each virtual location. Middle, two-dimensional autocorrelation of the cell's activity. Peaks in the autocorrelation function determined the spacing and angle of the fitted grid, which was then used to plot the estimated grid peaks (white x) across the entire environment. Right, cell spike waveform; red denotes mean. This cell had a gridness score of 0.51.

(b) The firing of a cell from participant 10's right entorhinal cortex (gridness score = 0.63).

(c,d) The firing of a different cell from participant 10's right entorhinal cortex in two consecutive sessions (gridness scores = 0.60 and 0.74).

(e) The activity of a different cell from participant 10's right entorhinal cortex (gridness score = 0.63).

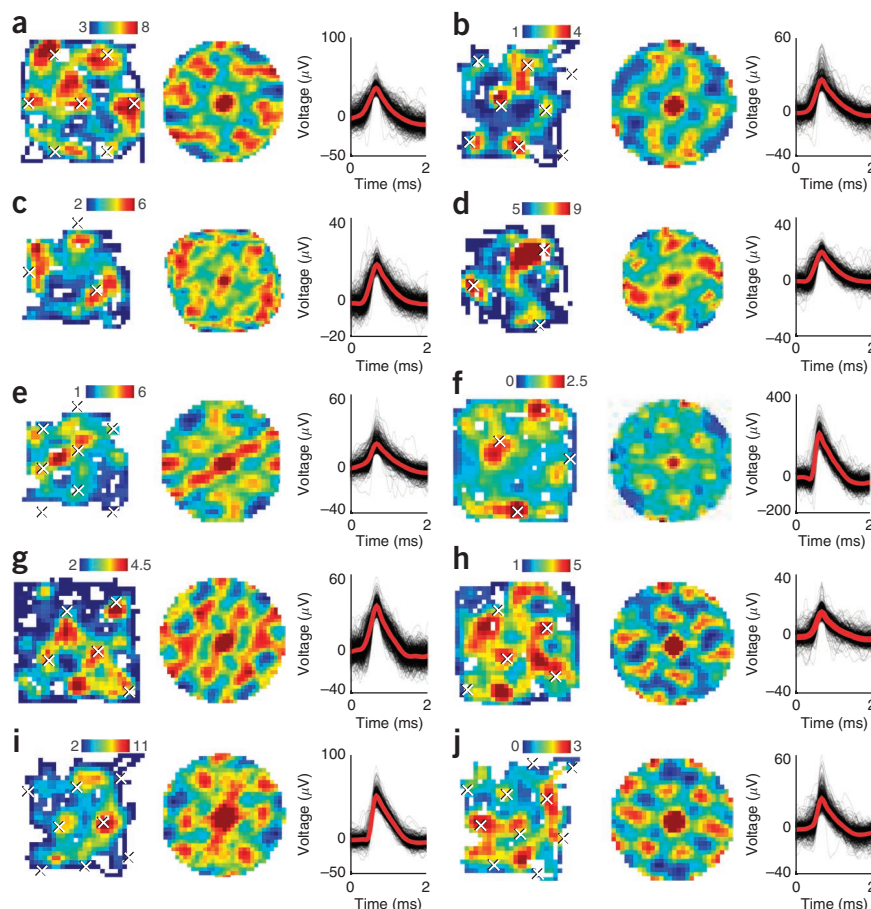
(f) The activity of a cell from participant 11's right cingulate cortex (gridness score = 0.67).

(g) The activity of a cell from participant 7's right cingulate cortex (gridness score = 0.51).

(h) The activity of a different cell from participant 7's right cingulate cortex (gridness score = 0.8).

(i) The activity of a cell from participant 10's right hippocampus (gridness score = 0.46).

(j) The activity of a cell from participant 10's right parahippocampal gyrus (gridness score = 0.72).



grid-like firing from other cells that activate at multiple spatial locations, such as multi-peaked place cells<sup>5</sup>. To measure the spatial arrangement between the locations represented by each cell's firing, we computed the two-dimensional spatial autocorrelation function for each cell's firing rate map. We found that the autocorrelation functions of many cells exhibited multiple distinct peaks that were arranged symmetrically (**Fig. 2** and **Supplementary Fig. 1**). In many cases, these patterns exhibited sixfold ( $60^\circ$ ) symmetry, indicating that the locations at which these cells activated were arranged in a triangular grid, similar to patterns observed in rodents<sup>7,10</sup>.

To identify cells with significant grid-like spatial firing, we computed each cell's gridness score, which quantifies the  $60^\circ$  periodicity in the cell's spatial autocorrelation function<sup>7</sup>. The gridness score was computed as the mean difference in the autocorrelation at the angles at which peaks would be expected in true grid cells ( $60^\circ$  and  $120^\circ$ ) compared with the angles at which troughs would be expected ( $30^\circ$ ,  $90^\circ$  and  $150^\circ$ ). A neuron was designated as exhibiting grid-like spatial firing if its gridness score was significantly greater than would be expected by chance ( $P < 0.05$ ; Online Methods).

We applied this grid identification procedure to each of the 893 cells in our data set, including cells from entorhinal cortex, hippocampus, amygdala, parahippocampal gyrus and cingulate cortex (**Fig. 3a**). Many cells exhibited significant grid-like activity. These cells were not uniformly distributed across brain areas ( $P < 0.001$ ,  $\chi^2$  test). The most grid-like cells were found in the entorhinal cortex and cingulate cortex, which consisted of 14% and 12% grid-like cells, respectively ( $P$  values  $< 0.0005$ , binomial tests; **Fig. 3b**). This peak proportion of grid-like cells in the entorhinal cortex is generally consistent with findings from human and animal studies<sup>7,9,11</sup>. There were also significant numbers of grid-like cells in the hippocampus (8%,  $P = 0.05$ ). There was no significant difference in the prevalence of grid-like cells between the right and left hemispheres ( $P > 0.5$ ,  $\chi^2$  test).

To verify that the sixfold rotational symmetry of grid-like cells is a distinctive feature of human neuronal coding, we tested for cells whose spatial firing exhibited four-, eight- or tenfold rotational symmetry. The eight- and tenfold symmetry analyses served as statistical control analyses, as grids with these angles do not tessellate. These analyses did not reveal significant numbers of cells exhibiting any symmetry type ( $P$  values  $> 0.01$ ; **Fig. 3c**) other than the six-way symmetry associated with grid cells. In particular, because we did not observe significant four-way rotational symmetry, we ruled out the possibility that the firing patterns could be driven by the square-like arrangement of the four objects.

Prior studies revealed detailed features of grid cells related to the spacing and direction-sensitivity of their representations<sup>7,10,11</sup>. Technical reasons precluded us from examining the relation between grid spacing and anatomical location of the recording electrode in the entorhinal cortex<sup>7,9</sup>. Comparing anterior and posterior cingulate, we found similar numbers of grid-like cells in each area (12% and 11% of cells in each respective region) and observed a trend in which cells in anterior cingulate had more widely spaced grids than cells in posterior cingulate ( $P = 0.1$ ). Of the cells exhibiting grid-like spatial firing, 18% exhibited an additional direction-related modulation (**Supplementary Table 1**), which is consistent with them exhibiting conjunctive grid-by-direction responses<sup>10</sup>. We found similar levels of grid-like spatial responses after statistically removing direction-related spiking activity, indicating that our findings of grid-like patterns were not artifacts of neural responses to direction or turning. We also conducted additional control analyses to confirm that the grid-like cells that we observed were stable over time (**Supplementary Fig. 2**) and not a result of multi-peaked place cells (**Supplementary Fig. 3**).

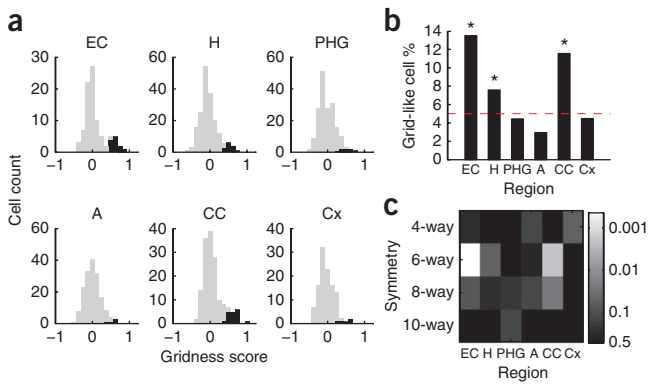


**Figure 3** Population measurements of cells exhibiting significant grid-like spatial firing. **(a)** The distribution of gridness scores from each region. Black bars indicate the gridness scores of cells that exhibited significant grid-like activity ( $P < 0.05$ ) and gray bars indicate other cells. A, amygdala; CC, cingulate cortex; Cx, frontal cortex; EC, entorhinal cortex; H, hippocampus; PHG, parahippocampal gyrus. **(b)** The proportion of significant grid-like cells across regions. Dashed line indicates the type 1 error rate (5%). Asterisks denote regions in which the observed number of cells exceeded the type 1 error rate at  $P < 0.01$  (binomial test). **(c)** The significance of cells exhibiting four-, six-, eight- and tenfold symmetric activity (binomial test).

In rodents, grid cells are part of a broader neuronal network related to spatial processing, including hippocampal place cells<sup>1,2</sup>. We identified place cells that had significantly elevated firing when the participant was at a specific virtual location (the cell's place field; **Supplementary Fig. 4a–d**). We observed significant levels of place cells in the hippocampus, parahippocampal gyrus and cingulate cortex ( $P$  values  $< 0.01$ ; **Supplementary Fig. 4e**). Consistent with recordings in animals navigating open environments, 80% of place cells did not significantly vary ( $P$  values  $> 0.05$ ) their firing rate in the place field according to the participant's heading; the remaining 20% of place cells were direction sensitive. We also tested for cells whose activity increased when the participant faced a particular virtual direction without necessarily encoding specific locations. Significant levels of direction-sensitive cells were found only in the hippocampus and parahippocampal gyrus (7% of cells in each region;  $P$  values  $< 0.03$ , binomial tests). Owing to the open environment in our task, the participant's direction correlates with viewing particular landmarks at the arena's boundaries. Thus, some apparent direction-sensitive cells may relate to viewing particular landmarks<sup>2,15</sup>. Finally, we tested for cells that represent combinations of linear regions of the environment<sup>16</sup>, but the results were inconclusive.

Our results demonstrate the existence of cells with grid-like spatial firing in the human brain and suggest that the human grid-cell network includes both entorhinal cortex and cingulate cortex. These results extend a growing body of findings in rodents<sup>7,10</sup> to humans and support the previous fMRI finding<sup>11</sup> of grid-like patterns in the human entorhinal cortex as well as in the frontal lobe (note that the cingulate cortex in which we found grid-like cells was posterior to the prefrontal areas reported previously<sup>11</sup>). Although it is difficult to extrapolate accurately from virtual to real-world movement, our estimate of the participants' perceived walking speeds ( $1.25\text{--}2\text{ m s}^{-1}$ , computed from the optic flow and their viewpoint height), suggests that individual grid cells have spacings between firing fields of at least 1–6 m in the physical world (extrapolating from the observed virtual grid spacings that spanned 27–84% of the environment's width; **Fig. 2**).

Although statistically robust, the grid-like cells that we observed had noisier firing maps than some grid cells reported in rodents. Scientists studying rodent grid cells generally target the dorsomedial entorhinal cortex precisely, but there is localization variability in epilepsy patients because neurosurgeons implant electrodes according to clinical needs<sup>12</sup>. It is also important to understand whether the activities of human grid-like cells are affected by other factors besides location, such as eye position<sup>9</sup>. An additional factor is that humans perform our virtual navigation task using only visual information and do not receive the proprioceptive feedback that occurs during normal locomotion and was shown to be important for accurate spatial representations in rodents<sup>17</sup>.

Given the purported role of the entorhinal cortex in spatial and nonspatial behaviors<sup>18,19</sup>, it seems likely that analogous grid-like signals also represent various types of human behavioral information. Thus, one important area of future research will be characterizing the information coding of these cells during non-navigational behaviors and the relation between grid cells, head-direction cells and eye movements<sup>9</sup>. The entorhinal cortex is the main input to the hippocampus, which is critical for episodic memory. Obtaining a better understanding of the behavior of widespread entorhinal cortex cells<sup>7,17,19,20</sup> is likely to shed light on how the human brain encodes spatial and nonspatial episodic memories in various contexts.

## METHODS

Methods and any associated references are available in the [online version of the paper](#).

*Note: Any Supplementary Information and Source Data files are available in the online version of the paper.*

## ACKNOWLEDGMENTS

We are grateful to the patients for participating in our study. We thank K. Lee, D. Wyeth, E. Wyeth, D. Pourshaban, E. Behnke and T. Fields for technical assistance. This work was supported by US National Institutes of Health grants MH061975 and NS033221.

## AUTHOR CONTRIBUTIONS

The experiment was designed by J.J., C.T.W., M.J.K., A.S. and I.F. Data were collected by J.J., C.T.W., J.E.M., J.F.B., I.E., M.R.S., A.D.S. and N.S. Data analyses were performed by J.J., X.-X.W., C.T.W., A.S. and M.J.K. J.J. and M.J.K. wrote the manuscript.

## COMPETING FINANCIAL INTERESTS

The authors declare no competing financial interests.

Reprints and permissions information is available online at <http://www.nature.com/reprints/index.html>.

- O'Keefe, J. & Dostrovsky, J. *Brain Res.* **34**, 171–175 (1971).
- Ekstrom, A.D. *et al. Nature* **425**, 184–188 (2003).
- McHugh, T.J. *et al. Cell* **87**, 1339–1349 (1996).
- Ulanovsky, N. & Moss, C. *Nat. Neurosci.* **10**, 224–233 (2007).
- Muller, R.U. *et al. J. Neurosci.* **7**, 1935–1950 (1987).
- Quirk, G.J. *et al. J. Neurosci.* **10**, 2008–2017 (1990).
- Hafting, T. *et al. Nature* **436**, 801–806 (2005).
- Yartsev, M.M. *et al. Nature* **479**, 103–107 (2011).
- Killian, N.J. *et al. Nature* **491**, 761–764 (2012).
- Sargolini, F. *et al. Science* **312**, 758–762 (2006).
- Doeller, C.F., Barry, C. & Burgess, N. *Nature* **463**, 657–661 (2010).
- Jacobs, J. & Kahana, M.J. *Trends Cogn. Sci.* **14**, 162–171 (2010).
- Jacobs, J. *et al. Proc. Natl. Acad. Sci. USA* **107**, 6487–6492 (2010).
- Bird, C.M. & Burgess, N. *Nat. Rev. Neurosci.* **9**, 182–194 (2008).
- Rolls, E.T. *Hippocampus* **9**, 467–480 (1999).
- Krupic, J., Burgess, N. & O'Keefe, J. *Science* **337**, 853–857 (2012).
- Terrazas, A. *et al. J. Neurosci.* **25**, 8085–8096 (2005).
- Buzsáki, G. & Moser, E. *Nat. Neurosci.* **16**, 130–138 (2013).
- Hargreaves, E.L. *et al. Science* **308**, 1792–1794 (2005).
- Tsao, A. *et al. Curr. Biol.* **23**, 399–405 (2013).

## ONLINE METHODS

**Task.** During free time between clinical procedures, patients performed a spatial learning task on a bedside laptop computer. Our testing protocol was approved by the institutional review boards of Thomas Jefferson University and the University of California, Los Angeles. In this task, participants learned the locations of four visible goal objects and then re-navigated to these locations with the objects invisible. At the beginning of each session, each of the four objects were shown sequentially on a black screen for 2,000 ms to familiarize the participants with their appearance; this was repeated five times. Participants were then placed in the virtual environment in which they began navigating, using a joystick to control the direction of their movement. In each trial, the participant was instructed to drive a virtual bicycle to the location of a randomly selected object. The virtual environment consisted of a large open square arena with visual cues that included textured walls, a panoramic background image and a floor that gradually transitioned between different colors. The participant's top speed of movement allowed them to travel between opposite walls of the environment in ~3.5 s. We defined the width of the environment as 28 virtual reality units (VRUs).

The beginning of each session was a training period to teach the participant the objects' locations. Each training trial began with the participant in the middle of the environment facing a single wall (north). Then they twice navigated to each object: the first time the object was clearly visible, and the second time, after being transported back to the center of the environment, the object was invisible until they were within 1.6 VRU. The participants visited each of the four objects in a random order, and then repeated this process three times for a total of 12 training trials. The objects were positioned in a large square-like shape (minor variations across sessions) to encourage participants to navigate throughout the environment (**Supplementary Fig. 5**).

After training, participants performed 48 delivery trials in which they were asked to navigate directly from one object location to another. The goal object remained invisible until the participant was very close to its location. In rare cases in which participants became disoriented, the experimenter could intervene to manually make the goal object appear. Participants navigated to each fixed goal location 12 times in a random order; there were approximately equal numbers of navigations between each pair of objects. We excluded seven sessions in which participants had poor navigation performance (defined as having a mean excess delivery path length greater than 100 VRU).

**Electrophysiology.** We recorded single-neuron spiking from 40- $\mu\text{m}$  research microwires that augmented the standard clinical macroelectrodes used by clinical teams to map epileptiform activity (**Supplementary Table 2**). Nine participants were recorded by I.F. using customized microelectrodes that extended from the tip of clinical depth electrodes. Five participants were recorded by A.D.S. using electrodes from AdTech that had microwires positioned on either the side or tip of each depth electrode. We localized electrodes by performing computed tomography scans after implant, aligning the computed tomography images with pre-implant MRIs (**Supplementary Fig. 6**), and then labeling the region of each electrode according to anatomical landmarks. We recorded electrical activity at 28–32 kHz and identified spikes from individual cells using wavelet clustering and temporal autocorrelations<sup>21</sup>. The amplitude of individual spike waveforms averaged 48  $\mu\text{V}$  (**Supplementary Table 3**). Our accuracy in distinguishing individual cells and background noise was largely consistent with recordings from animals, as measured using standard methods<sup>22</sup>: 76% of cells had a false-negative error rate less than 10% and 82% had an error rate less than 20%. 78% of cells had a false-positive error rate less than 10% and 85% had an error rate less than 20%.

**Data analysis.** Our data analyses probed the relation between each cell's firing rate and the participant's location in the virtual environment. We excluded cells with mean firing rates below 0.5 Hz or above 10 Hz (potential interneurons).

We divided each recording session into 50-ms epochs and excluded any time intervals when the participant was not moving. Then, we computed the firing rate of each neuron across the environment, binning this activity into a  $28 \times 28$  array and excluding any locations that were not occupied for at least 100 ms (24% of the environment excluded on average). This firing-rate map was then smoothed with a  $5 \times 5$  gaussian kernel<sup>7</sup>.

To characterize the spatial firing of each neuron, we computed the spatial autocorrelation,  $r$ , of each neuron's smoothed firing rate<sup>7</sup>. This function identifies spatial patterns in the cell's firing by computing the correlation between the firing rates at positions  $(x, y)$  and  $(x - \tau_x, y - \tau_y)$ , aggregating across all locations  $(x, y)$  in the environment

$$r(\tau_x, \tau_y) = \frac{n \sum_{x,y} \lambda(x,y) \lambda(x - \tau_x, y - \tau_y) - \sum_{x,y} \lambda(x,y) \sum_{x,y} \lambda(x - \tau_x, y - \tau_y)}{\sqrt{\left( n \sum_{x,y} \lambda(x,y)^2 - \left( \sum_{x,y} \lambda(x,y) \right)^2 \right) \left( n \sum_{x,y} \lambda(x - \tau_x, y - \tau_y)^2 - \left( \sum_{x,y} \lambda(x - \tau_x, y - \tau_y) \right)^2 \right)}}$$

where  $\tau_x$  and  $\tau_y$  correspond to spatial lags,  $\lambda(x,y)$  is the firing rate at array location  $(x,y)$ , and  $n$  corresponds to the number of valid observations for  $(x,y)$ ,  $(x - \tau_x, y - \tau_y)$ . To minimize potential spurious patterns, we only computed  $r(\tau_x, \tau_y)$  for values  $(\tau_x, \tau_y)$  with at least 20 observations.

Using this autocorrelation function, we then computed each neuron's gridness score<sup>10</sup> as the correlation ( $\text{cor}$ ) between the elements in the original autocorrelation matrix  $r$  and a series of rotated autocorrelation matrices  $r^\theta$  where  $\theta$  is the angle of rotation. Each cell's gridness score,  $g$ , was thus determined as

$$g = \min(\text{cor}(r, r^{60^\circ}), \text{cor}(r, r^{120^\circ})) - \max(\text{cor}(r, r^{30^\circ}), \text{cor}(r, r^{90^\circ}), \text{cor}(r, r^{150^\circ}))$$

We computed each cell's gridness score as the maximum  $g$  across radii  $L \in 5 \dots 28$ , in each computation including only  $r(\tau_x, \tau_y)$  such that  $5 \leq \sqrt{x^2 + y^2} \leq L$ .

We used a permutation procedure to identify putative grid cells by comparing each cell's observed gridness score,  $g$ , with the distribution of gridness scores expected by chance for that cell,  $g^*$ . To estimate  $g^*$  for each cell, we reshuffled the original spiking data 1,000 times and, for each shuffle, computed the gridness scores exactly as described above. This reshuffling preserved the temporal correlations in the participant's behavior and neural activity by randomly rotating the spiking data with a circular wraparound. We designated a neuron as a putative grid cell if its true gridness score exceeded 95% of the distribution of  $g^*$  and was positive. To identify cells exhibiting four-, eight- or tenfold symmetric firing (**Fig. 3c**), we followed an analogous procedure but instead used appropriate angles when computing  $g$ . For example, for fourfold symmetry, we used

$$g = \min(\text{cor}(r, r^{90^\circ})) - \max(\text{cor}(r, r^{45^\circ}), \text{cor}(r, r^{135^\circ}))$$

To identify place cells, we used  $t$  tests to compare the firing rate within 5 VRUs of each virtual location with the activity at other locations<sup>13</sup>. A neuron was designated as a place cell if its smallest location-related  $P$  value was less than observed from reshuffled data at  $P < 0.05$ . This procedure used the time-shifting reshuffling described above and thus it was unlikely for a significant place cell to be caused by only a single traversal of a given location. We identified direction-sensitive place cells by using an ANOVA to determine if the cell's firing inside the place field significantly varied according to the cardinal direction the participant faced.

21. Quiroga, R.Q. *et al. Neural Comput.* **16**, 1661–1687 (2004).

22. Hill, D.N., Mehta, S. & Kleinfeld, D. *J. Neurosci.* **31**, 8699–8705 (2011).